Inorganic Chemistry

Article

Cite This: Inorg. Chem. 2017, 56, 14842−14849

pubs.acs.org/IC

Investigation of a Structural Phase Transition and Magnetic Structure of $Na_2BaFe(VO_4)_2$: A Triangular Magnetic Lattice with a Ferromagnetic Ground State

Liurukara D. Sanjeewa,[†] Vasile O. Garlea,[‡] Michael A. McGuire,[§] Matthias Frontzek,[‡] Colin D. McMillen,[†] Kyle Fulle,[†] and Joseph W. Kolis*[,†]

[†]Department of Chemistry and Center for Optical Materials Science and Engineering Technologies (COMSET), Clemson University, Clemson, South Carolina 29634-0973, United States

[‡]Neutron Scattering Division, Oak Ridge National Laboratory, Oak Ridge, Tennessee 37831, United States

[§]Materials Science and Technology Division, Oak Ridge National Laboratory, Oak Ridge, Tennessee 37831, United States

Supporting Information

ABSTRACT: The structural and magnetic properties of a glaserite-type $Na_2BaFe(VO_4)_2$ compound, featuring a triangular magnetic lattice of Fe^{2+} ($S = 2$), are reported. Temperature dependent X-ray single crystal studies indicate that at room temperature the system adopts a trigonal $P\bar{3}m1$ structure and undergoes a structural phase transition to a $C2/c$ monoclinic phase slightly below room temperature (T_s = 288 K). This structural transition involves a tilting of Fe−O−V bond angles and strongly influences the magnetic correlation within the Fe triangular lattice. The magnetic susceptibility measurements reveal a ferromagnetic transition near 7 K. Single crystal neutron diffraction confirms the structural distortion and the ferromagnetic spin ordering in $Na_2BaFe(VO_4)_2$. The magnetic structure of the ordered state is modeled in the magnetic space group $C2'/c'$ that implies a ferromagnetic order of the a and c moment components and antiferromagnetic arrangement for the b components. Overall, the Fe magnetic moments form ferromagnetic layers that are stacked along the c-axis, where the spins point along one of the (111) facets of the FeO_6 octahedron.

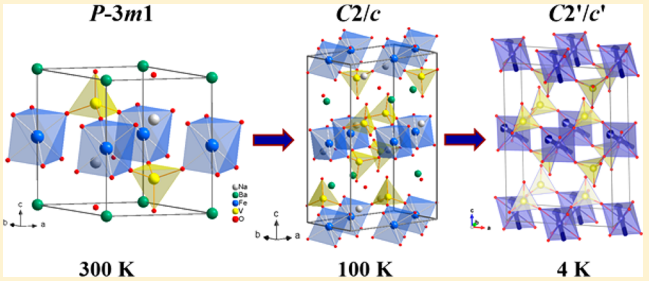

1. INTRODUCTION

The vanadate oxyanion, $(VO_4)^{3-}$, has proven to be an exceptionally versatile and interesting building block in solids containing first row transition metal complexes. The unit can adopt a wide range of structural environments leading to a large number of new compounds.[1,2] Because of the vacant d-orbitals on the vanadium center, vanadates display a range of unusual magnetic coupling behavior.[3−8] When this structural versatility and magnetic complexity are combined, some interesting solid-state effects can occur.[9,10] The tetrahedral bridging group can also introduce 3-fold symmetry, leading to spin frustration,[11−13] which further increases the magnetic complexity.[14] It is well-known that extensive vanadate chemistry is obtained from low temperature (ca. 200 °C) hydrothermal synthesis.[15] More recently we found that the high temperature hydrothermal growth method is an excellent route to new transition metal vanadates.[16−19] Hydrothermal reactions at 500−600 °C in concentrated hydroxide or halide mineralizers not only generate a wide range of new phases but also lead to the growth of large, high quality single crystals. In many cases these crystals can be sufficiently large to enable measurements such as single crystal neutron diffraction. Our recent work has focused on a series of low dimensional metal vanadates that adopt one of three structure types of naturally occurring minerals, namely, descloizite,[20] brackebuschite,[21] and glaserite.[22]

In particular, the transition metal−vanadate glaserite structure type has demonstrated considerable complexity in both its physical and magnetic phases. Structurally there are a number of phase transitions that occur from the ideal $P\bar{3}m1$ space group to lower symmetry monoclinic phases.[23] It is known that these phase transitions can be very subtle but can have a considerable effect on the resultant magnetic properties (*vide infra*). The structural flexibility of the glaserite phase enables a wide range of substitution of metals ions of various sizes, oxidation states, and spin states. As such it can be described as a widely adaptable structure type.[24] The trigonal symmetry adopted in the higher symmetry glaserites can lead to frustrated spin states, making them a particularly interesting group to study.

Vanadate glaserite materials based on first row transition metals can be broadly described by the formula of $A_2A'M(VO_4)_2$, where A = monovalent cation, Li^+, Na^+, K^+, or Ag^+, A′ = either monovalent or divalent cation, Ag^+, Sr^{2+}, or Ba^{2+}, and M = divalent or trivalent magnetic d-block cation, Co^{2+}, Mn^{2+},

Received: August 10, 2017
Published: December 7, 2017

DOI: 10.1021/acs.inorgchem.7b02024
Inorg. Chem. 2017, 56, 14842−14849

Ni^{2+}, or Fe^{3+}. In the case where A = alkali cation and A′ = Ag^{+}, or both A and A′ are Ag^{+}, then M can be trivalent iron (Fe^{3+}).[25,26] Much more commonly, however, A′ is a divalent alkaline earth ion where the transition metal ion is a divalent species Co^{2+}, Mn^{2+}, or Ni^{2+}.[27,28] There is a range of structure types adopted by the general glaserite formula, and they appear to be highly sensitive to the identity of the alkali and alkaline earth cations.[23] In general it has been observed that, when A′ = Sr^{2+}, the room temperature structure is in a monoclinic space group ($P2/m$ or $C2/c$), but when A′ = Ba, the room temperature structure is in a trigonal space group ($P\bar{3}$ or $P\bar{3}m1$).[22,27−31] In the most extreme case of $BaAg_2Cu(VO_4)_2$, where there is significant Jahn−Teller distortion, a completely different structure with triclinic symmetry is observed.[32] In all these structures, the magnetic ions are arranged on a 2D regular triangular lattice with layers well separated from one another by nonmagnetic A and A′ cations. The 2D triangular lattice is constructed from corner sharing MO_6 octahedra and VO_4 tetrahedra, where the isolated octahedral sites are bridged through the tetrahedral linkers. The structural variations affecting the space group symmetry also impact the magnetic structures. In most cases involving divalent transition metals studied thus far (Co^{2+}, Mn^{2+}, Ni^{2+}), long-range magnetic order, such as ferromagnetism, is often observed at low temperature regardless of the initial room temperature crystal symmetry. Previous workers observed different magnetic properties of the $BaAg_2M(VO_4)_2$ and $SrAg_2M(VO_4)_2$, M = Co^{2+} and Ni^{2+}, series due to the tilting of the vanadate groups compared to the MO_6 octahedra. The authors emphasize that the M−O−V angle can have a signficiant influence on magnetic superexchange via empty d-orbitals of the VO_4 groups.[27,28,33,34]

To our knowledge, there have not been any reported studies of the magnetic behavior of divalent iron glaserites. The only previously reported example of a Fe^{2+} glaserite $Na_2BaFe(VO_4)_2$ that we are aware of was reported by our group synthesized by a hydrothermal method.[22] This is in contrast to the previous work that employed higher temperature flux methods that appear to favor the higher oxidation state Fe^{3+} ion.[25,26] The ability to grow single crystals of $Na_2BaFe(VO_4)_2$ allows for the detailed investigation of the magnetic properties of an S = 2 glaserite phase. In this case the parent compound displays unique phase transition behavior in that it adopts a trigonal $P\bar{3}m1$ phase at room temperature, but undergoes a structural phase transition to a $C2/c$ phase slightly below room temperature (288 K), along with magnetic phase transitions at lower temperature. This is unlike the previously reported Co^{2+}, Ni^{2+}, and Mn^{2+} examples that display a variety of magnetic phase transitions at relatively low temperatures (ca. ≤10 K) but do not appear to display any other structural transitions between those temperatures and room temperature. To our knowledge no previous work demonstrated a clear-cut *structural* transition in a glaserite phase as temperatures are reduced from ambient to 2 K. This paper describes the first magnetic study of Fe^{2+} in a glaserite phase as well as a structural phase transition at 288 K from a trigonal to monoclinic as well as magnetic phase change at 6.7 K, mostly ferromagnetic in nature. The single crystals were large enough that the magnetically ordered structure was also studied by single crystal neutron diffraction.

2. EXPERIMENTAL SECTION

Single crystals of $Na_2BaFe(VO_4)_2$ were grown using a high temperature, high pressure hydrothermal technique. In a typical reaction, Na_2CO_3 (Aldrich, 99%), BaO (AlfaAesar, 99.5%), Fe_2O_3 (Alfa Aesar, 99.99%), and V_2O_5 (Alfa Aesar, 99.6%) were mixed in a molar ratio of 2:1:1:2. Specifically, a total of 0.2 g of reactants (Na_2CO_3 (0.0477 g); BaO (0.0345 g); Fe_2O_3 (0.0359); and V_2O_5 (0.0819 g)) was mixed with 0.4 mL of 5 M NaOH in a 2.5 in. long 1/4 in. diameter silver ampule. After the reactants and the mineralizer were loaded, the silver ampules were sealed and heated in a Tuttle-seal autoclave filled with water to provide suitable counter pressure at 580 °C for 2 weeks. After the reaction time, hexagonal black crystals of 2 mm in size were isolated after aqueous rinse.[22]

Single crystal X-ray diffraction was performed at a range of temperatures (300 to 100 K) to investigate the structural phase transition of $Na_2BaFe(VO_4)_2$. X-ray data was collected using a Bruker D8 Venture instrument equipped with an Incoatec Mo Kα microfocus source (λ = 0.71073 Å) and Photon 100 CMOS detector. The structures were solved by intrinsic phasing and refined by full-matrix least-squares techniques on F^2 using the SHELXTL software package.[35] Results of the structure refinements, positional parameters, and selected interatomic distances and angles are summarized in Tables 1−3.

Table 1. Structure Refinements of $Na_2BaFe(VO_4)_2$ at 300 and 100 K Determined by Single Crystal X-ray Diffraction

empirical formula	$Na_2BaFe(VO_4)_2$	$Na_2BaFe(VO_4)_2$
fw	469.05	469.05
cryst syst	trigonal	monoclinic
cryst dimens, mm	0.099 × 0.089 × 0.067	0.099 × 0.089 × 0.067
space group, Z	$P\bar{3}m1$ (No. 164), 1	$C2/c$ (No. 15), 4
T, K	300	100
a, Å	5.5680(4)	9.5534(6)
b, Å		5.6033(6)
c, Å	7.1030(5)	14.1249(11)
β, deg		90.332(4)
V, Å^3	190.71(3)	756.10(11)
D (calc, g/cm^3)	4.072	4.120
F(000)	214	856
T_{max}, T_{min}	1.000, 0.6647	1.000, 0.5986
2θ range	5.11−26.45	2.88−28.00
no. of unique reflns	168	916
no. of params	21	67
final R [$I > 2\sigma(I)$] R1, wR2	0.0316/0.0839	0.0489/0.1172
final R (all data) R1, wR2	0.0316/0.0839	0.0492/0.1173
GOF	1.165	1.150
largest diff peak/hole, e/Å^3	1.181/−0.992	4.4185/−5.894
μ(Mo Kα), mm^{-1}	9.428	9.539

Temperature and magnetic field dependent magnetization data were collected using a Quantum Design Magnetic Property Measurement System. Measurements over the temperature range of 2 to 380 K were conducted on a single crystal with the dimensions of 2.2 × 1.6 × 0.4 mm with the magnetic field parallel and perpendicular to the hexagonal c-axis. Higher temperature data, up to 780 K, were collected using a collection of several non-coaligned crystals.

Single crystal neutron diffraction data were collected using a HB3A four-circle diffractometer at High Flux Isotope Reactor in Oak Ridge National laboratory.[36] The same single crystal specimen as used in the magnetization study was used to conduct the measurements. The crystal was glued onto an aluminum pin and loaded into a closed-cycle refrigerator whose temperature can be controlled within the range of 300 to 4 K. A monochromatic beam of 1.542 Å was selected using a multilayer-[110]-wafer silicon monochromator, and the scattered intensity was measured using an Anger-camera type detector. The neutron diffraction data were analyzed by using the FullProf Suite Package.[37]

DOI: 10.1021/acs.inorgchem.7b02024
Inorg. Chem. 2017, 56, 14842−14849

Table 2. Atomic Positional Parameters of $Na_2BaFe(VO_4)_2$ from Single Crystal X-ray Diffraction

atom	Wyckoff pos	x	y	z
		$P\bar{3}m1$ (300 K)		
Na(1)	2d	−1/3	1/3	−0.3338(9)
Ba(1)	1a	0	0	0
Fe(1)	1b	0	0	1/2
V(1)	2d	−2/3	2/3	−0.2342(3)
O(1)	2d	−1/3	1/3	−0.0021(13)
O(2)	6i	0.3384(15)	0.1692(8)	0.3166(10)
		$C2/c$ (100 K)		
Na(1)	8f	0.3313(4)	0.4710(7)	0.0845(3)
Ba(1)	4e	1/2	−0.0558(15)	1/4
Fe(1)	4b	1/2	0	1/2
V(1)	8f	0.3325(2)	0.4722(3)	0.3680(2)
O(1)	8f	0.3238(8)	0.5138(14)	0.2502(5)
O(2)	8f	0.3870(7)	0.7343(13)	0.4197(5)
O(3)	8f	0.4510(7)	0.2471(13)	0.3968(5)
O(4)	8f	0.1710(7)	0.4022(13)	0.4121(5)

Table 3. Selected Interatomic Distances (Å) and Angles (deg) of $Na_2BaFe(VO_4)_2$ from Single Crystal X-ray Diffraction

$P\bar{3}m1$		$C2/c$	
	$Fe(1)O_6$		
Fe(1)−O(2) × 6	2.088(7)	Fe(1)−O(2) × 2	2.158(7)
		Fe(1)−O(3) × 2	2.063(7)
		Fe(1)−O(4) × 2	2.126(7)
	$V(1)O_4$		
V(1)−O(1)	1.678(10)	V(1)−O(1)	1.682(7)
V(1)−O(2) × 3	1.688(7)	V(1)−O(2)	1.719(7)
Fe(1)−O(2)−V(1)	161.7(4)	V(1)−O(3)	1.741(7)
		V(1)−O(4)	1.717(7)
		Fe(1)−O(3)−V(1)	164.1(4)
		Fe(1)−O(4)−V(1)	148.0(4)

3. RESULTS AND DISCUSSION

3.1. Crystal Structure and Phase Transition of $Na_2BaFe(VO_4)_2$. X-ray structural investigations on $Na_2BaFe(VO_4)_2$ reveal a structural transition just below room temperature, around 290 K, where the structure transforms from trigonal, $P\bar{3}m1$, at high temperatures to monoclinic, $C2/c$, at low temperatures. The unit cell parameters of the trigonal phase are a = 5.5680(4) Å and c = 7.1030(5) Å, V = 190.71(3) Å^3, Z = 1, and those of the monoclinic phase are a = 9.5534(6) Å, b = 5.6033(6) Å, and c = 14.1249(11) Å with β = 90.332(4)°, V = 756.10(11) Å^3, Z = 4. Both structure types are reported previously in the literature for different compounds, but to our knowledge a phase transition between these two structure types has not been elucidated for an individual compound. However, it is interesting to note that the alkali rare earth glaserite, $K_3Y(VO_4)_2$, was separately indexed in space group $C2/c$ by powder diffraction,[38] and $P\bar{3}m1$ by single crystal diffraction,[39] and it may be that small differences in the room temperature of the two studies in Moscow, Russia, and South Carolina, USA, straddles a similar phase transition to what is observed in $Na_2BaFe(VO_4)_2$ in the present study.

The descent in symmetry of the phase transition leads to variations in the bond lengths and angles, breaking the rigid trigonal symmetry, but similar general structural motifs are observed in both phases. The general structure of $Na_2BaFe(VO_4)_2$ consists of a two-dimensional Fe−O−V lattice where Na^+ ions are located in gaps within the transitional vanadate layers, and Ba^{2+} ions are located between the transition metal vanadate layers (Figures 1a and 1b). This 2D Fe−O−V lattice

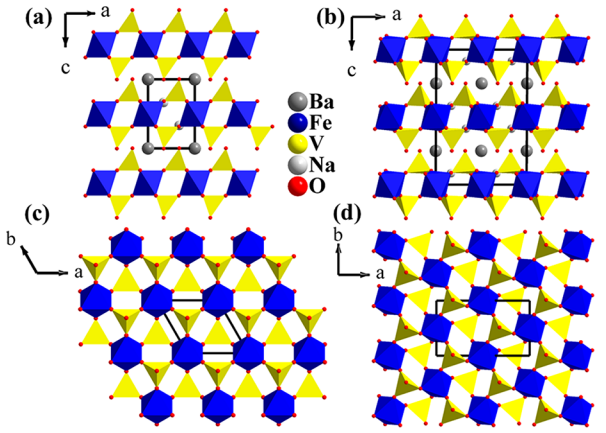

Figure 1. Polyhedral view of the $Na_2BaFe(VO_4)_2$ trigonal (a, c) and monoclinic (b, d) structure types: panels a and b show the stacking of Fe−O−V layers along the c-axis for both trigonal and monoclinic structures viewed along the b-axis; panels c and d show the relative orientation of the FeO_6 and VO_4 groups in the 2D Fe−O−V layers, accentuating the tilting relative to the c-axis.

is composed of FeO_6 octahedra and VO_4 tetrahedra. Each FeO_6 octahedron connects to three VO_4 tetrahedra via basal oxygen atoms, creating a triangular Fe lattice along the ab-plane (Figures 1c, 1d, 2a, 2b). The subtle structural differences in the

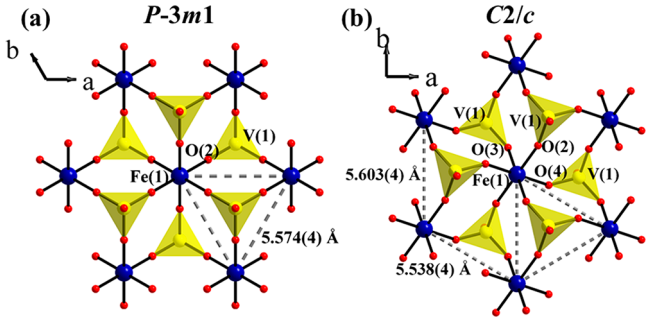

Figure 2. Relative orientation of FeO_6 and VO_4 groups in trigonal (a) and monoclinic (b) structures having slight differences in the triangular Fe lattices.

trigonal and monoclinic structure types are important to note in order to account for the observed magnetic properties. A detailed structural description of the trigonal phase is given in ref 22. The FeO_6 octahedra in trigonal $Na_2BaFe(VO_4)_2$ are undistorted with Fe(1)−O(1) of 2.088(7) Å, and the VO_4 tetrahedra only show a slight variation (remaining within the uncertainties) in V(1)−O distances to the two unique oxygen atoms (1.678(10) Å to 1.688(7) Å). As a result, the octahedral FeO_6 units (symmetry D_{3d}) forms a perfect planar triangular lattice, as shown in Figure 2a. The monoclinic $C2/c$ structure is a distortion of the trigonal $P\bar{3}m1$ structure in which the two nonequivalent oxygen atomic positions in the trigonal structure type are split into four distinct sites in the monoclinic phase. Therefore, the local symmetries of the Fe and V sites are distorted, with the FeO_6 symmetry reduced from D_{3d} to C_i and

DOI: 10.1021/acs.inorgchem.7b02024
Inorg. Chem. 2017, 56, 14842−14849

the VO_4 symmetry reduced from C_{3v} to C_1. In the monoclinic structure, the Fe(1)−O bond distances range from 2.062(7) Å to 2.157(7) Å and V(1)−O range from 1.682(7) Å to 1.741(7) Å. The resulting Fe−Fe triangular lattice is distorted in the monoclinic structure, and though it remains planar in the *ab*-plane, Figure 2b, the Fe atoms form isosceles triangles with Fe−Fe distances of 5.538(4) Å and 5.603(4) Å.

Another key difference is the Fe−O−V bond angles of the two structures. For example, in the trigonal structure the Fe−O−V bond angle is 161.7(4)°, and in the monoclinic structure the Fe−O−V angles are 164.1(4)° and 148.0(4)°. In particular the Fe(1)−O(4)−V(1) bond angle (148.0(4)°) induces a tilting of the FeO_6 and VO_4 units within the monoclinic 2D Fe−O−V lattice compared to the trigonal 2D Fe−O−V layers. The relative orientation of FeO_6 and VO_4 can be considered as the key component for the magnetic properties of $Na_2BaFe(VO_4)_2$. In this structure there are no direct Fe−O−Fe bridges, so all the magnetic coupling (superexchange pathway) is probably through the empty d-orbital of V^{5+} ions. Thus, the Fe−O−V bond angle is particularly important to the type and degree of magnetic exchange, making such subtle details of the structural phases significant. The ordered nature of the $P\bar{3}m1$ structure and the tilting of the octahedra and tetrahedra in the $C2/c$ structure suggests that the phase transition is not simply an order/disorder transition. This phase transition is also somewhat reminiscent of phase transitions that occur in $KFe(MoO_4)_2$ (which has similar lattice parameters to the title compound, but is not a glaserite structure type) where the structure also distorts slightly from ideal $P\bar{3}m1$ to $C2/c$ at 311 K.[40] In contrast to $KFe(MoO_4)_2$, however, where there are two unique Fe atoms at lower symmetry, each with two coupling constants, there is still only one unique iron site at the lower symmetry in the system reported herein.

3.2. Magnetic Properties of $Na_2BaFe(VO_4)_2$. Results of magnetization (M) measurements on a single crystal of $Na_2BaFe(VO_4)_2$ are summarized in Figure 3. Data were collected for the magnetic field (H) applied parallel to the *c*-axis (normal to the triangular layers) and perpendicular to the *c*-axis (within the triangular layers). The main panel of Figure 3a shows the temperature dependence of M/H. The main feature is the rapid upturn upon cooling that occurs at low temperature, shown over a narrower temperature range in Figure 3b. Isothermal magnetization curves above and below this transition are shown in the inset of Figure 3a. At 2 K, M increases rapidly with applied field to about 2.5 μ_B/Fe, and then continues to increase almost linearly as the field is increased further. Both the temperature and field dependence of M indicate a strong ferromagnetic component to the magnetic phase transition at ∼7 K, comparable to that determined by neutron scattering discussed below. However, the reduced saturation magnetization component, relative to the 4 μ_B estimated for divalent iron (S = 2), and the observed linear increase in M at higher fields indicate a more complex magnetic structure, also discussed in more detail below.

It can be noted in Figure 3a that a small ferromagnetic component is also present in M vs H data near room temperature. Measurements of M vs H curves at temperatures up to 780 K (not shown) indicate that this arises from a ferromagnetic impurity with Curie temperature near 850 K. This Curie temperature, the size of the measured moment, and the observation of a subtle anomaly near 120 K in M vs T suggest the sample contains about 1 wt % of Fe_3O_4.

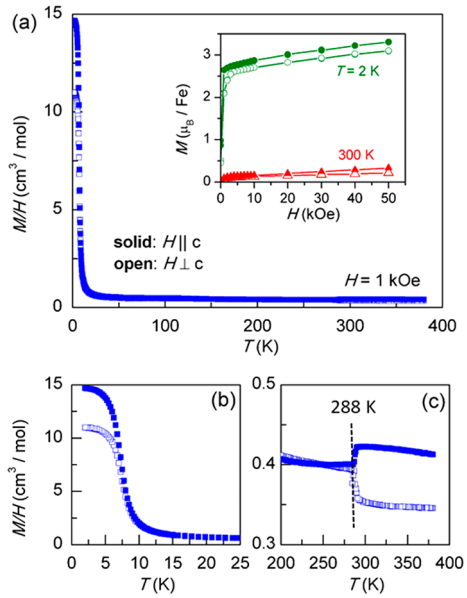

Figure 3. Magnetization data for $Na_2BaFe(VO_4)_2$. Temperature dependence of M/H between 2 and 350 K is shown in panel a, with M vs H curves measured at 2 and 300 K in the inset. The temperature dependence near the magnetic ordering and crystallographic phase transitions is shown in panels b and c, respectively.

The paramagnetic susceptibility of $Na_2BaFe(VO_4)_2$ was determined by the slope of the M vs H curves (neglecting the ferromagnetic offset from Fe_3O_4) measured between 200 and 780 K. Curie−Weiss fits to this data give an effective moment per iron of 5.1(1) μ_B and a small Weiss temperature of 18(2) K. The effective moment is typical for high spin Fe^{2+}, which often has an orbital contribution in addition to the 4.8 μ_B spin-only value, and the positive Weiss temperature indicates predominately ferromagnetic interactions. Additionally, a magnetic anomaly is observed at the crystallographic phase transition. This is shown in Figure 3c. Upon cooling from the trigonal to the monoclinic phase, the magnetization along the *c*-axis decreases and the magnetization in the *ab*-plane increases. Though the detailed origin of this behavior is unclear, it is likely related to differences in magnetocrystalline anisotropy in the two structures arising from spin−orbit coupling. Thermal hysteresis of about 10 K was observed between data collected on warming and cooling, consistent with a first order crystallographic phase transition.

3.3. Magnetic Structure of $Na_2BaFe(VO_4)_2$. Neutron diffraction measurements were conducted over the temperature range of 300 to 4 K. The change of crystal structure from trigonal ($P\bar{3}m1$) to monoclinic ($C/2c$) was also evidenced in the single crystal neutron diffraction experiment. The (−2,0,2) Bragg peak shows a significant broadening and a decrease in intensity between 300 and 295 K, while additional scattering is detected at the (−2,1,1/2) peak position confirming the doubling of *c*-axis below the structural transformation, Figure 4a,b.

A systematic survey of the reciprocal space was performed at the lowest measured temperature, 4 K, in order to detect the presence of magnetic scattering associated with the long-range magnetic order observed in the magnetization measurement. Scans along the (0,0,L) direction, shown in Figure 4c, revealed an increase in intensity for the $(0,0,1/2)_{trig}$ and $(0,0,3/2)_{trig}$ reflections. Note that the indexing of the peak position in this

DOI: 10.1021/acs.inorgchem.7b02024
Inorg. Chem. 2017, 56, 14842−14849

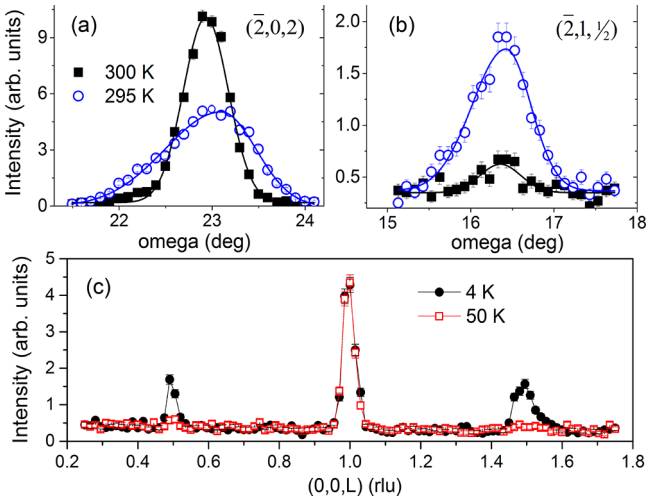

Figure 4. (a) Structural transformation indicated by the broadening of the trigonal (−2,0,2) peak between 300 and 295 K. (b) Increase in scattering at the (−2,1,1/2) peak, which demonstrates the doubling of the crystal periodicity along the *c*-axis, $c_{mono} = 2c_{trig}$. (c) Scans along the (0,0,*L*) direction revealing the appearance of $(0,0,L = (2n + 1)/2)_{trig}$ magnetic reflections at 4 K.

figure corresponds to the trigonal unit cell. When indexed using the monoclinic unit cell ($c_{mono} = 2c_{trig}$) these reflections become $(0,0,1)_{mon}$ and $(0,0,3)_{mon}$ while the magnetic propagation vector is **k** = (0,0,0). The order parameter of the magnetic transition was determined by following the temperature dependence of the $(-1,1,0)_{trig}$ and $(0,0,3/2)_{trig}$ peak intensities. As displayed in Figure 5, the order parameter curves follow a power-law dependence and indicate the onset of magnetic long-range order at approximately 6.7 K, in agreement with the magnetization data.

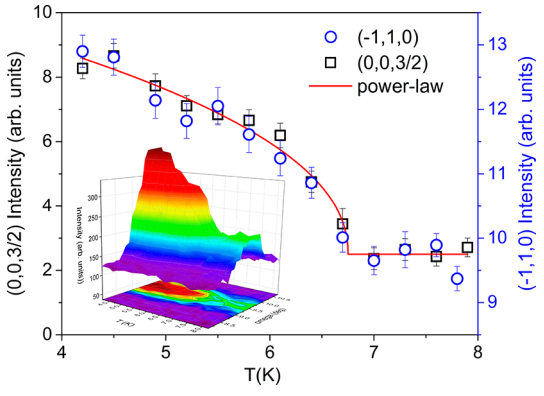

Figure 5. Temperature dependence of the $(-1,1,0)_{trig}$ and $(0,0,3/2)_{trig}$ magnetic peak integrated intensities from neutron scattering. The red line represents a power-law fit to the order parameter data yielding a T_c of 6.7(2) K. The inset shows a 3D plot of the omega scans at the (0,0,3/2) peak position performed at different temperatures around the magnetic transition.

In order to separate the magnetic from the nuclear contribution, we first performed a structural refinement using the diffraction data collected at 50 K. For this we employed the crystal structure model based on the monoclinic space group *C*2/*c* obtained with the X-ray diffraction at 100 K (Table 1). The so achieved structural parameters, which included the atomic positions, thermal parameters, and extinction coefficient, were fixed for the combined nuclear and magnetic refinement of the 4 K data. Possible magnetic models allowed by the crystal symmetry were explored using the tools available at the Bilbao Crystallographic Server.[41,42] There are two maximal magnetic space groups for monoclinic *C*2/*c* and **k** = (0 0 0) propagation vector, that allow ordered moments on the Fe site (Wyckoff 4b): *C*2′/*c*′ (#15.89) and *C*2/*c* (#15.85). The *C*2′/*c*′ space group implies a ferromagnetic order of the *a* and *c* moment components and antiferromagnetic order for the *b* components, and gives the best description of the experimental data. The Fe atomic coordinates and the corresponding magnetic moment sequence are $(0,1/2,0|m_a,m_b,m_c)$, $(0,1/2,1/2|m_a,-m_b,m_c)$, $(1/2,0,0|m_a,m_b,m_c)$, and $(1/2,0,1/2|m_a,-m_b,m_c)$. It is worth noting that this model is in excellent agreement with the magnetization data that suggested the presence of FM components both along the *c*-axis and in the *ab*-plane.

The restrained nuclear and magnetic refinement using 126 distinct reflections collected at 4 K data gave an R_F factor of 14.3% and χ^2 of 4.95. A comparison of the calculated and observed structure factors along with the estimated magnetic contribution for each reflection is shown in Figure 6. The

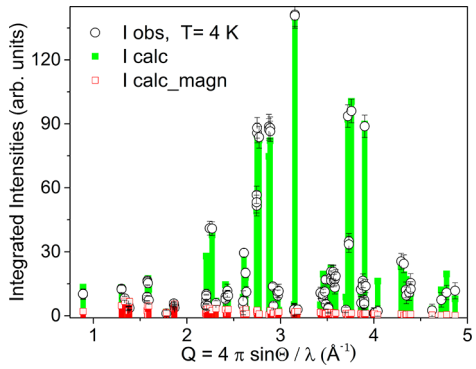

Figure 6. Comparison of the observed neutron scattering intensities at 4 K and calculated intensities using the nuclear and magnetic structure model described in the text. The magnetic contribution to the calculated values for each reflection is depicted by red.

refined moments are $m_a = -1.8(3)\ \mu_B$, $m_b = 3.6(2)\ \mu_B$, and $m_c = 2.5(3)\ \mu_B$, yielding a total amplitude of $4.8(3)\ \mu_B$, larger than the expected spin-only value for *S* = 2. As noted in the previous section, orbital angular momentum is not quenched for Fe^{2+} so there is a significant orbital contribution expected to the total moment. The proposed magnetic structure model is shown in Figure 7. The Fe magnetic moments form ferromagnetic layers, where all the spins are parallel pointing along one of the (111) facets of the FeO_6 octahedron. These layers are stacked along the *c*-direction by alternating their magnetic moments around the *b*-direction to produce a net magnetization in the *ac*-plane (see Figure 7b).

4. SUMMARY AND CONCLUSION

The unusual structural and magnetic properties of a Fe^{2+} glaserite phase $Na_2BaFe(VO_4)_2$ are reported. The triangular lattice structures using $[VO_4]^{3-}$ as a bridging unit building block have attracted considerable investigation since they often exhibit complex magnetic behavior. The glaserite structure in general provides a rich field of study in this regard. For example, in $AAg_2Fe(VO_4)_2$, A = K and Rb, containing trivalent Fe^{3+}, the 3-fold symmetry of the magnetic lattice was preserved without a structural distortion caused by any phase transition.

DOI: 10.1021/acs.inorgchem.7b02024
Inorg. Chem. 2017, 56, 14842−14849

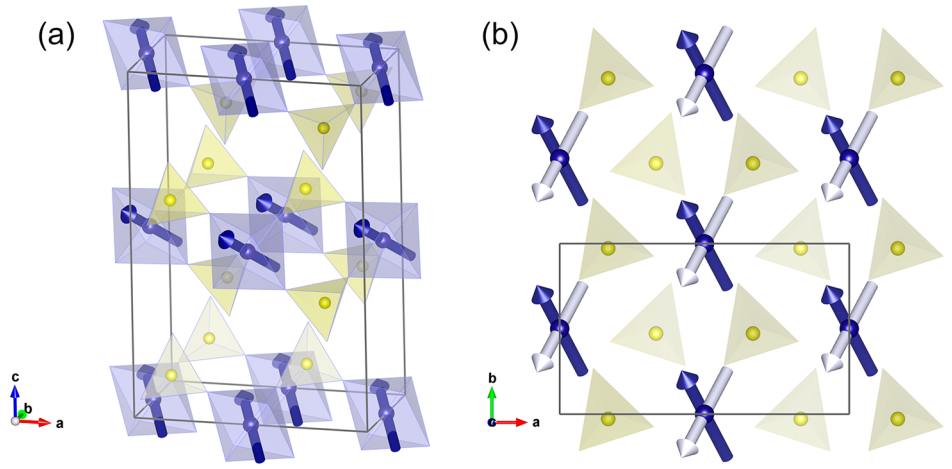

Figure 7. (a) Schematic view of the magnetic structure of $Na_2BaFe(VO_4)_2$ at 4 K. (b) view of the magnetic structure along the *c*-direction. The magnetic moments of Fe are aligned parallel to form ferromagnetic layers that are stacked along the *c*-axis. Successive layers are alternating their moment directions along the *b*-direction (silver and blue vectors), while the *a* and *c* components remain ferromagnetically aligned, leading to a net magnetization in the *ac*-plane.

Glaserites containing other divalent metal ions Mn^{2+}, Co^{2+}, and Ni^{2+} adopt either trigonal or monoclinic *C*2/*c* structures at room temperature depending on the identity of the alkaline earth ion in the lattice. Interestingly, the Co^{2+} and Ni^{2+} examples display magnetic ordering below 10 K but no structural transition regardless of the room temperature structure. In contrast, the Mn^{2+} species displays antiferromagnetic ordering at low temperature, while again there is no evidence of a structural phase transition regardless of room temperature structure. However, in this study, the first example of a divalent iron glaserite, $Na_2BaFe(VO_4)_2$ shows a structural transition from trigonal $P\bar{3}m1$ to monoclinic *C*2/*c* as confirmed from single crystal structure studies from room temperature to 100 K. This structural phase transition distorts the local symmetry of FeO_6 octahedra and VO_4 tetrahedra in $Na_2BaFe(VO_4)_2$ thereby tilting the Fe−O−V bonds compared to the room temperature structure. This distortion could induce an anisotropy in the magnetic triangular lattice, which subsequently leads to the observed ferromagnetic ordering below 10 K.

The Ba analogues of the divalent transition metals ($BaAg_2M(VO_4)_2$, M = Mn^{2+}, Co^{2+}, Ni^{2+}) also adopt the trigonal symmetry displayed by $Na_2BaFe(VO_4)_2$ at room temperature. To our knowledge no low temperature single crystal structural study has been reported on these compounds to examine structural phase transitions, but the magnetic studies do not suggest any structural phase transitions similar to those observed here in $Na_2BaFe(VO_4)_2$. The trigonal structure type is also present in $AAg_2Fe(VO_4)_2$ (containing trivalent iron), and it retains the trigonal structure to low temperatures and displays evidence of spin frustrated behavior. In contrast, the room temperature structures of $SrAg_2M(VO_4)_2$ (M = Mn^{2+}, Co^{2+}, Ni^{2+}) share similar structural features with the low temperature structure of $Na_2BaFe(VO_4)_2$, adopting *C*2/*c* symmetry and showing a similar distortion in the Fe−O−V 2D lattices. They also adopt ferromagnetic ordering below 10 K. Therefore, $Na_2BaFe(VO_4)_2$ is an interesting intermediate example that adopts ferromagnetic ordering at 6.7 K but undergoes a structural phase change below room temperature, making it a good candidate to test the role of structural phase transitions versus magnetic ordering in the glaserite type.

■ ASSOCIATED CONTENT

Supporting Information

The Supporting Information is available free of charge on the ACS Publications website at DOI: 10.1021/acs.inorgchem.7b02024.

Synthesized X-ray precession photographs at 300 and 100 K (PDF)

Accession Codes

CCDC 1567343−1567344 contain the supplementary crystallographic data for this paper. These data can be obtained free of charge via www.ccdc.cam.ac.uk/data_request/cif, or by emailing data_request@ccdc.cam.ac.uk, or by contacting The Cambridge Crystallographic Data Centre, 12 Union Road, Cambridge CB2 1EZ, UK; fax: +44 1223 336033.

■ AUTHOR INFORMATION

Corresponding Author

*E-mail: kjoseph@clemson.edu.

ORCID

Michael A. McGuire: 0000-0003-1762-9406

Colin D. McMillen: 0000-0002-7773-8797

Notes

The authors declare no competing financial interest.

■ ACKNOWLEDGMENTS

The authors thank the National Science Foundation for financial support, Grant No. DMR-1410727. Work at the Oak Ridge National Laboratory was sponsored by the Scientific User Facilities Division (neutron diffraction) and Materials Sciences and Engineering Division (magnetization measurements), Office of Basic Energy Sciences, US Department of Energy (DOE).

■ REFERENCES

(1) Zavalij, P. Y.; Whittingham, M. S. Structural Chemistry of Vanadium Oxides with Open Frameworks. *Acta Crystallogr., Sect. B: Struct. Sci.* **1999**, *55*, 627−663.

(2) Schindler, M.; Hawthorne, F. C.; Baur, W. H. A Crystal-chemical Approach to the Composition and Occurrence of Vanadium Minerals. *Can. Mineral.* **2000**, *38*, 1443−1456.

DOI: 10.1021/acs.inorgchem.7b02024
Inorg. Chem. 2017, 56, 14842−14849

(3) Lawes, G.; Harris, A. B.; Kimura, T.; Rogado, N.; Cava, R. J.; Aharony, A.; Entin-Wohlman, O.; Yildirim, T.; Kenzelmann, M.; Broholm, C.; Ramirez, A. P. Magnetically Driven Ferroelectric Order in $Ni_3(VO_4)_2$. *Phys. Rev. Lett.* **2005**, *95*, 087205.
(4) Bellido, N.; Martin, C.; Simon, C.; Maignan, C. A. Coupled Negative Magnetocapacitance and Magnetic Susceptibility in a Kagomé Staircase-like Compound $Co_3V_2O_8$. *J. Phys.: Condens. Matter* **2007**, *19*, 056001.
(5) Ben Yahia, H.; Gaudin, E.; Boulahya, K.; Darriet, J.; Son, W.-J.; Whangbo, M.-H. Synthesis and Characterization of the Crystal Structure and Magnetic Properties of the Ternary Manganese Vanadate $NaMnVO_4$. *Inorg. Chem.* **2010**, *49*, 8578−8582.
(6) Clemens, O.; Rohrer, J.; Nenert, G. Magnetic Structures of the Low Temperature Phase of $Mn_3(VO_4)_2$ − Towards Understanding Magnetic Ordering Between Adjacent Kagomé Layers. *Dalton Trans.* **2016**, *45*, 156−171.
(7) Niesen, S. K.; Heyer, O.; Lorenz, T.; Valldor, M. Antiferromagnetic Heisenberg S= 5/2 Spin Chain Compound $SrMn_2V_2O_8$. *J. Magn. Magn. Mater.* **2011**, *323*, 2575−2578.
(8) He, Z.; Ueda, Y.; Itoh, M. Magnetic Properties of the Quasi-one-dimensional System $BaMn_2V_2O_8$. *Solid State Commun.* **2007**, *141*, 22−24.
(9) Sun, K.; Litvinchuk, A. P.; Tapp, J.; Lorenz, B.; Möller, A. $BaMn_9(VO)_6(OH)_2$: A Unique Canted Antiferromagnet with a Chiral "Paddle-Wheel" Structural Feature. *Inorg. Chem.* **2015**, *54*, 898−904.
(10) Sanjeewa, L. D.; McGuire, M. A.; McMillen, C. D.; Willett, D.; Chumanov, G.; Kolis, J. W. Honeycomb-like S = 5/2 Spin Lattices in New Manganese(II) Vanadates. *Inorg. Chem.* **2016**, *55*, 9240−9249.
(11) Greedan, J. E. Geometrically Frustrated Magnetic Materials. *J. Mater. Chem.* **2001**, *11*, 37−53.
(12) Ramirez, A. P. Strongly Geometrically Frustrated Magnets. *Annu. Rev. Mater. Sci.* **1994**, *24*, 453−480.
(13) Dai, D.; Whangbo, M. H. Classical Spin and Quantum-mechanical Descriptions of Geometric Spin Frustration. *J. Chem. Phys.* **2004**, *121*, 672−680.
(14) Freedman, D. E.; Chisnell, R.; McQueen, T. M.; Lee, Y. S.; Payen, C.; Nocera, D. G. Frustrated Magnetism in the S= 1 Kagome lattice $BaNi_3(OH)_2(VO_4)_2$. *Chem. Commun.* **2012**, *48*, 64−66.
(15) Chirayil, T.; Zavalij, P. Y.; Whittingham, M. S. Hydrothermal Synthesis of Vanadium Oxides. *Chem. Mater.* **1998**, *10*, 2629−2640.
(16) McMillen, C. D.; Kolis, J. W. Hydrothermal Synthesis as a Route to Mineralogically-Inspired Structures. *J. Chem. Soc., Dalton Trans.* **2016**, *45*, 2772−2784.
(17) Sanjeewa, L. D.; McMillen, C. D.; McGuire, M. A.; Kolis, J. W. Manganese Vanadate Chemistry in Hydrothermal BaF_2 Brines: $Ba_3Mn_2(V_2O_7)F_2$ and $Ba_7Mn_8O_2(VO_4)_2F_{23}$. *Inorg. Chem.* **2016**, *55*, 12512−12515.
(18) Smith Pellizzeri, T. M.; McMillen, C. D.; Wen, Y.; Chumanov, G.; Kolis, J. W. Three Unique Barium Manganese Vanadates from High-Temperature Hydrothermal Brines. *Inorg. Chem.* **2017**, *56*, 4206−4216.
(19) Sanjeewa, L. D.; McGuire, M. A.; McMillen, C. D.; Garlea, V. O.; Kolis, J. W. Polar Materials with Isolated V^{4+} S = 1/2 triangles: $Na_2Sr_2V_3O_3(Ge_4O_{13})Cl$ and $K_2Sr_2V_3O_3(Ge_4O_{13})Cl$. *Chem. Mater.* **2017**, *29*, 1404−1412.
(20) Sanjeewa, L. D.; McGuire, M. A.; McMillen, C. D.; Willett, D.; Chumanov, G.; Kolis, J. W. Honeycomb-like S = 5/2 Spin Lattices in New Manganese (II) Vanadates. *Inorg. Chem.* **2016**, *55*, 9240−9249.
(21) Sanjeewa, L. D.; McGuire, M. A.; Garlea, O. V.; Hu, L.; Chumanov, G.; McMillen, C. D.; Kolis, J. W. Hydrothermal Synthesis and Characterization of Brackebuschite-type Transition Metal Vanadate: $Ba_2M(VO_4)_2(OH)$, M = V^{3+}, Mn^{3+} and Fe^{3+}. *Inorg. Chem.* **2015**, *54*, 7014−7020.
(22) Sanjeewa, L. D.; McMillen, C. D.; Willett, D.; Chumanov, G.; Kolis, J. W. Hydrothermal Synthesis of Single Crystals of Transition Metal Vanadates in the Glaserite Phase. *J. Solid State Chem.* **2016**, *236*, 61−68.
(23) Nikolova, R.; Kostov-Kytin, V. Crystal Chemistry of "Glaserite" Type Compounds. *Bulg. Chem. Commun.* **2013**, *45*, 418−426.
(24) Smit, J. P.; Stair, P. C.; Poeppelmeier, K. R. The Adaptable Lyonsite Structure. *Chem. - Eur. J.* **2006**, *12*, 5944−5953.
(25) Amuneke, N. E.; Tapp, J.; de la Cruz, C. R.; Möller, A. Experimental Realization of a Unique Class of Compounds: XY-Antiferromagnetic Triangular Lattices, $KAg_2Fe[VO_4]_2$ and $RbAg_2Fe[VO_4]_2$, with Ferroelectric Ground States. *Chem. Mater.* **2014**, *26*, 5930−5935.
(26) Becht, G. A.; Vaughey, J. T.; Hwu, S. J. $Ag_3Fe(VO_4)_2$ and $AgFeV_2O_7$: Synthesis, Structure, and Electrochemical Characteristics of Two New Silver Iron (III) Vanadates. *Chem. Mater.* **2009**, *22*, 1149−1154.
(27) Möller, A.; Amuneke, N. E.; Daniel, P.; Lorenz, B.; de la Cruz, C. R.; Gooch, M.; Chu, P. C. $AAg_2M[VO_4]_2$ (A= Ba, Sr; M= Co, Ni): A Series of Ferromagnetic Insulators. *Phys. Rev. B: Condens. Matter Mater. Phys.* **2012**, *85*, 214422.
(28) Bratsch, M.; Tapp, J.; Litvinchuk, A. P.; Möller, A. $AAg_2(M'_{1/3}M_{2/3})[VO_4]_2$: Synthesis, Magnetic Properties, and Lattice Dynamics of Honeycomb-Type Lattices. *Inorg. Chem.* **2014**, *53*, 4994−5001.
(29) Nakayama, G.; Hara, S.; Sato, H.; Narumi, Y.; Nojiri, H. Synthesis and Magnetic Properties of a New Series of Triangular-lattice Magnets, $Na_2BaMV_2O_8$ (M= Ni, Co, and Mn). *J. Phys.: Condens. Matter* **2013**, *25*, 116003.
(30) Rettich, R.; Müller-Buschbaum, H. Zur Kristallchemie der Silber-Mangan-Oxovanadate $Ag_2BaMnV_2O_8$ und $(AgCa_2)Mn_2(VO_4)_3$/On the Crystal Chemistry of the Silver Manganese Oxovanadates $Ag_2BaMnV_2O_8$ and $(AgCa_2)Mn_2(VO_4)_3$. *Z. Naturforsch., B* **1998**, *53b*, 291−295.
(31) Rettich, R.; Müller-Buschbaum, H. Ag^+ als Substituent Eines Alkalimetalls in $Ag_2SrMnV_2O_8$/Ag^+ as Substituent of an Alkaline Metal in $Ag_2SrMnV_2O_8$. *Z. Naturforsch., B* **1998**, *53b*, 279.
(32) Amuneke, N. E.; Gheorghe, D. E.; Lorenz, B.; Möller, A. Synthesis, Crystal Structure and Physical Properties of $BaAg_2Cu[VO_4]_2$: A New Member of the S = 1/2 Triangular Lattice. *Inorg. Chem.* **2011**, *50*, 2207−2214.
(33) Möller, A.; Schmitt, M.; Schnelle, W.; Förster, T.; Rosner, H. $AgCuVO_4$: A quasi-one-dimensional S = 1/2 chain compound. *Phys. Rev. B: Condens. Matter Mater. Phys.* **2009**, *80*, 125106.
(34) Tsirlin, A. A.; Möller, A.; Lorenz, B.; Skourski, Y.; Rosner, H. Superposition of ferromagnetic and antiferromagnetic spin chains in the quantum magnet $BaAg_2Cu[VO_4]_2$. *Phys. Rev. B: Condens. Matter Mater. Phys.* **2012**, *85*, 014401.
(35) Sheldrick, G. M. A. Short History of SHELX. *Acta Crystallogr., Sect. A: Found. Crystallogr.* **2008**, *64*, 112−122.
(36) Chakoumakos, B. C.; Cao, H. B.; Ye, F.; Stoica, A. D.; Popovici, M.; Sundaram, M.; Zhou, W.; Hicks, J. S.; Lynn, G. W.; Riedel, R. Four-circle Single-crystal Neutron Diffractometer at the High Flux Isotope Reactor. *J. Appl. Crystallogr.* **2011**, *44*, 655−658.
(37) Rodriguez-Carvajal, J. Recent Advances in Magnetic Structure Determination by Neutron Powder Diffraction. *Phys. B* **1993**, *192*, 55−69. Program available at https://www.ill.eu/sites/fullprof/.
(38) Bobylev, A. P.; Boubentsova, M. N.; Komissarova, L. N.; Ogorodova, L. P.; Spiridonov, F. M. Synthesis, Structure and Properties of a Double Potassium-yttrium Vanadate. *Mendeleev Commun.* **2004**, *14*, 146−147.
(39) Kimani, M. M.; Thompson, L.; Snider, W.; McMillen, C. D.; Kolis, J. W. Hydrothermal Synthesis and Spectroscopic Properties of a New Glaserite Material, $K_3RE(VO_4)_2$ (RE = Sc, Y, Dy, Ho, Er, Yb, Lu, or Tm) with Potential Lasing and Optical Properties. *Inorg. Chem.* **2012**, *51*, 13271−13280.
(40) Maczka, M.; Pietraszko, A.; Saraiva, G. D.; Souza Filho, A. G.; Paraguassu, W.; Lemos, V.; Perottoni, C. A.; Gallas, M. R.; Freire, P. T. C.; Tomaszewski, P. E.; Melo, F. E. A.; Mendes Filho, J.; Hanuza, J. High Pressure Effects on the Structural and Vibrational Properties of Antiferromagnetic KFe(MoO4)2. *J. Phys.: Condens. Matter* **2005**, *17*, 6285−6300.
(41) Gallego, S. V.; Tasci, E. S.; de la Flor, G.; Perez-Mato, J. M.; Aroyo, M. I. Magnetic Symmetry in the Bilbao Crystallographic Server: A Computer Program to Provide Systematic Absences of

DOI: 10.1021/acs.inorgchem.7b02024
Inorg. Chem. 2017, 56, 14842−14849

Magnetic Neutron Diffraction. *J. Appl. Crystallogr.* **2012**, *45*, 1236−1247.
(42) Perez-Mato, J. M.; Gallego, S. V.; Tasci, E. S.; Elcoro, L.; de la Flor, G.; Aroyo, M. I. Symmetry-Based Computational Tools for Magnetic Crystallography. *Annu. Rev. Mater. Res.* **2015**, *45*, 217−248. Server is available at http://www.cryst.ehu.es.

DOI: 10.1021/acs.inorgchem.7b02024
Inorg. Chem. 2017, 56, 14842−14849